HUANG LIANSHENG et al. Preprint of the conference manuscript

Next-Generation Coil Power Supply System for the Tokamak: Design, Implementation, and Operational Performance

HUANG Liansheng, CHEN Xiaojiao, ZHANG Xiuqing, HE Shiying, DOU Sheng, WANG Zejing, LI Lingpeng, ZUO Ying

Institute of Plasma Physics, Chinese Academy of Sciences

Hefei, China

Email: huangls@ipp.ac.cn

Abstract

In order to enhance the plasma confinement and overall performance of the Tokamak machine, an advanced poloidal field coil power supply system is developed in this study based on the pulsed power endogenous supply design concept, which is the first system of its kind to adopt fully controlled power electronics and pulsed power modulation technology, and utilizes a three-phase PWM rectifier plus H-bridge scheme based on fully controlled IGBTs to realize a four-quadrant output. The response time of the output voltage will be shortened from the commutation cycle time of the thyristor power supply to the switching cycle time of the IGBT, further improving the output response capability. In addition, the front-stage PWM rectifier combined with the phase-shifting transformer on the input side performs carrier phase shifting, which can optimize power quality and meet the requirements of system operation. At present, two sets of next-generation EAST poloidal field coil power supplies have been successfully constructed and have undergone more than two years of EAST operation, supporting 403 seconds and 1066 seconds long-pulse high-power H-mode operations. The next-generation power supplies operate stably and meet the design expectations, providing a theoretical basis and technical support for the design and construction of higher-power voltage-source coil power supplies in the future.

1. INTRODUCTION

EAST is a type of tokamak device. Both the toroidal magnetic field (TF) and the poloidal field (PF) coils are made of superconducting materials. The PF system, which includes the central solenoid, comprises 14 superconducting coils powered by 12 independent power supplies. The operational voltage and current requirements for the PF coils were determined through analysis of three nominal plasma configurations (elongated, circular, and large-volume) while accounting for the voltage demands for plasma current, position, and shape control. Each EAST PF power supply unit integrates alternating current/direct current (AC/DC) converters, a switch network unit (SNU), and a quench protection (QP) circuit. A distributed control system (DCS) is implemented for comprehensive monitoring and control of all PF power supply parameters. The SNU functions to insert discharge resistors into the tokamak magnet circuit, enabling dissipation of the stored magnetic energy from the coils. The fundamental QP configuration consists of a thyristor bypass circuit, two fast-opening switches, a pyro-breaker serving as a backup switch, discharge resistors, and fuses.

The coil power supply serves as a critical subsystem in tokamak fusion devices, being solely responsible for achieving high-temperature plasma ignition, ohmic heating, and plasma shape control. Its performance directly determines the operational capability and stability of the entire tokamak system. Currently, thyristor converters are widely employed in poloidal field power supplies (PFPS) of tokamak facilities[1], such as ITER[2], HL-2A[3], J-TEXT[4], and JT-60SA[5], owing to the high voltage and current handling capacity of thyristors. These systems are typically fed by flywheel generators or directly from the grid[6]. Nevertheless, thyristor-controlled converters (TCSC) exhibit inherent limitations, including slow dynamic response, significant harmonic distortion, and limited power efficiency[7][8]. In recent years, three-level PWM converters utilizing fully controlled semiconductor devices have gained increasing adoption in high-power applications. With the growing maturity of fully controlled power device technology and notable improvements in power ratings, next-generation voltage-source magnetic coil power supplies based on these devices demonstrate superior performance in terms of current harmonic suppression, power factor correction, and dynamic response compared to conventional thyristor-based systems. This paper presents the development of an advanced power supply for the poloidal field coils of the EAST tokamak, utilizing fully controlled converter technology.

The next-generation voltage-source poloidal field magnetic coil power supply utilizes IGBTs as the power switching devices and features a cascaded configuration comprising a front-end three-phase PWM converter and a rear-end H-bridge converter, as illustrated in Fig. 1. In comparison with conventional two-level PWM converters, the three-level topology offers two distinct advantages: firstly, each switching device withstands only half of the total DC-link voltage, thereby significantly reducing the voltage stress requirements; secondly, the synthesized output voltage waveform exhibits superior harmonic characteristics with improved sinusoidal

IAEA-FEC-2025 / INDICO ID 3240

Preprint of the conference manuscript

quality on the AC side, leading to substantially reduced harmonic distortion [9]. The IGBT modules, capable of active turn-on and turn-off operations and incorporating anti-parallel diodes, provide inherent bidirectional current flow capability. This configuration establishes the fundamental hardware foundation for achieving full four-quadrant output operation.

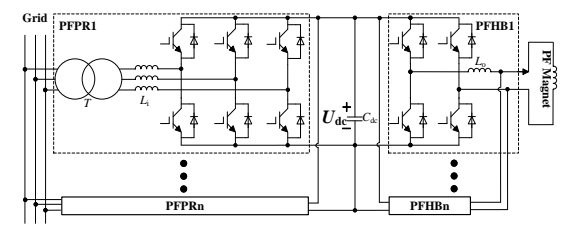


Fig. 1. Topology Scheme of EAST Voltage-Source Type Poloidal Field Coil Power Supply

The three-phase PWM converter draws power from the AC bus through a rectifier transformer and delivers a regulated DC voltage to supply the subsequent H-bridge converter. On the DC side, the H-bridge converter operates to switch this stable DC input into the dynamically variable voltage required by the magnetic coil load. Consequently, the output voltage response time is substantially reduced—from the commutation period typical of thyristor-based supplies to the switching cycle duration of the H-bridge IGBTs—thereby significantly enhancing the dynamic response capability of the system. The front-end three-phase PWM converter implements orthogonal current control in the synchronous rotating reference frame (d-q frame), which ensures nearly unity power factor and low input current harmonic distortion. This study focuses on the EAST poloidal field coil power supply as a platform for developing a next-generation voltage-source power supply. A systematic design methodology for key parameters is established, followed by the construction and commissioning of two full-scale prototype units. Detailed operational analysis validates the performance and feasibility of the proposed approach..

2. ANALYSIS OF THE RELATIONSHIP BETWEEN CURRENT HARMONICS AND PARAMETERS

2.1. Current Harmonic Analysis

RMS value of the harmonic components in the secondary-side phase current over a switching period is defined as the switching-period harmonic current, denoted as his_{Ts} . T The average of these RMS values over a fundamental frequency period is defined as the average harmonic current, denoted as his_{av} , which serves as a metric for evaluating the harmonic performance of the secondary-side phase current.

Based on the vector relationship at the AC side of the three-phase PWM converter, Equation (1) can be derived. In this equation, ω represents the fundamental angular frequency, $E_{\rm sm}$ is the fundamental amplitude of the secondary side phase voltage, which equals the fundamental amplitude of the secondary side line voltage divided by $\sqrt{3}$. $I_{\rm smej}$ indicates the rated fundamental amplitude of the secondary-side branch phase current under the condition of branch rated power $P_{\rm ej}$. Furthermore, $U_{\rm me}$ is the fundamental frequency amplitude of the rated phase bridge arm voltage, which is the fundamental frequency amplitude $U_{\rm m}$ of the phase bridge arm voltage when the fundamental frequency amplitude of the secondary branch phase current is equal to $I_{\rm smej}$. $m_{\rm e}$ is the rated modulation index when $U_{\rm m}$ equals $U_{\rm me}$.

$$U_{\text{me}} = \sqrt{E_{\text{sm}}^2 + (I_{\text{sme}}\omega L_{\text{i}})^2} = m_{\text{e}} \frac{U_{\text{de}}}{2}$$

$$\frac{3E_{\text{sm}}I_{\text{smej}}}{2} = P_{\text{ej}}$$
(1)

According to Equation (1), under the condition of constant branch power P_{ej} , U_{me} is influenced by E_{sm} and L_i , and Equation (1) can be rewritten as follows.

$$\begin{cases} U_{\rm me}^2 = E_{\rm sm}^2 + \frac{4(P_{\rm ej}\omega L_{\rm i})^2}{9E_{\rm sm}^2} \\ E_{\rm smmin}^2 = \frac{2P_{\rm ej}\omega L_{\rm i}}{3} \end{cases} \tag{2}$$
 The effective value of primary-side phase current harmonics $hip_{\rm av}$ is introduced to measure the harmonic level

The effective value of primary-side phase current harmonics hip_{av} is introduced to measure the harmonic level of the primary side phase current. In the case of a single branch, hip_{av} can be directly converted from the transformer turns ratio, as shown in Equation (3). Here, E_{pm} represents the fundamental amplitude of the primary side phase voltage.

HUANG LIANSHENG et al.

Preprint of the conference manuscript

$$hip_{sY_av} = \frac{his_{sY_av}E_{sm}}{E_{pm}}$$
 (3)

In this section, L_{ipu} [10] is introduced as the per-unit value of L_i , and its expression is given as follows.

$$L_{\rm ipu} = \frac{4P_{\rm ej}\omega}{3U_{\rm me}^2} L_{\rm i} \tag{4}$$

By introducing L_{ipu} , it allows the relationship between the primary-side current harmonics hip_{av} and modulation index m_e to be established without dependence on U_{dc} , decoupling the harmonic control from loss control. In summary, the mutual influences between the variables are summarized in Table 1.

TABLE 1. The mutual influence relationships between variables

Condition	Subcase	Regulatory means	Regulatory results
	$E_{\rm sm} < E_{\rm smmin}$	$U_{me} {\uparrow}$	$hip_{_{\mathrm{av}}}\!\!\downarrow$
$L_{ m i}$ -	$E_{\rm sm} > E_{\rm smmin}$	$U_{me} {\uparrow}$	$hip_{ m av}^{} \uparrow$
	None	$m_{ m e} \uparrow$	$hip_{ m av} \downarrow$
U_{me} -	$E_{\rm sm} < E_{\rm smmin}$	$L_{ m i} {\uparrow}$	$hip_{ m av}^{} \uparrow$
	$E_{\rm sm} > E_{\rm smmin}$	$L_{ m i} {\uparrow}$	$hip_{_{\mathbf{a}\mathrm{V}}}\!\!\downarrow$

The principles for analyzing output current harmonics are the same as those for input current harmonics. Since the poloidal field magnetic coil inductance is relatively large, this paper will not elaborate further.

2.2. Loss Analysis

Among the total power losses in the converter system, IGBT power devices constitute the dominant portion. The losses in each IGBT module comprise two primary components: conduction losses and switching losses. The rated conduction loss of the IGBT, denoted as P_{lce} , can be expressed by Equation (5) based on the technical manual fitting.

$$P_{\text{lce}} \approx \begin{cases} \text{PWM converter: } U_{\text{thr}} \left(\frac{2.4U_{\text{dc}}}{U_{\text{igbtr}}}\right)^{0.5} I_{\text{smej_av}} + r_{r} I_{\text{igbtr}} I_{\text{smej_rms}} \left(\frac{2.4U_{\text{dc}}}{U_{\text{igbtr}}}\right)^{0.357} \\ \text{H-bridge converter: } U_{\text{thr}} \left(\frac{2.4U_{\text{dc}}}{U_{\text{igbtr}}}\right)^{0.5} I_{\text{oej_av}} + r_{r} I_{\text{igbtr}} I_{\text{oej_rms}} \left(\frac{2.4U_{\text{dc}}}{U_{\text{igbtr}}}\right)^{0.357} \end{cases}$$

$$(5)$$

For the PWM converter, $I_{\text{smej_av}}$ is the half-wave average value of I_{smej} , and $I_{\text{smej_rms}}$ is the effective value of I_{smej} . According to the sine wave characteristics, the relationship between $I_{\text{smej_av}}$, $I_{\text{smej_rms}}$, and I_{smej} is given by Equation (6).

$$\begin{cases} I_{smej_av} = \frac{2I_{smej}}{\pi} \\ I_{smej_rms} = \frac{I_{smej}}{\sqrt{2}} \\ I_{oej_av} = I_{oej} \\ I_{oej_rms} = I_{oej} \end{cases}$$

$$(6)$$

Based on Equations (5) and (6), the power device losses of the PWM converter are positively correlated with the DC voltage $U_{\rm dc}$ and the fundamental amplitude of the secondary side branch phase current $I_{\rm smej}$. The relationship between $U_{\rm dc}$ and $I_{\rm smej}$ is shown in Equation (7).

$$I_{\rm smej} = \frac{4P_{\rm ej}}{3m_{\rm e}U_{\rm dc}} \sqrt{\frac{2}{1 \pm \sqrt{1 - L_{\rm ipu}^2}}}$$
 (7)

Switching losses are obtained by multiplying the energy loss of each switching action by the switching frequency. The energy loss can also be fitted from the technical manual. The relationship between power device losses and power supply parameters is summarized in Table 2., where P_{lse} represents the rated switching loss, and P_{lte} represents the rated total loss.

TABLE 2. Relationship between power device losses of PWM converter and adjustment of power supply parameters

Condition Success Regulatory means Regulatory results of 1 (1) converter	Condition	Subcase	Regulatory means	Regulatory results of PWM converter
--	-----------	---------	------------------	-------------------------------------

IAEA-FEC-2025 / INDICO ID 3240 Preprint of the conference manuscript

$m_{\rm e}$ -, $L_{ m ipu}$ -	None	$U_{ m dc} \! \uparrow$	$P_{\text{lce}}\downarrow$, P_{lse} -, $P_{\text{lte}}\downarrow$
$U_{ m dc}$ -	None	$m_{ m e} \uparrow$	$P_{\rm lce} \downarrow, P_{\rm lse} \downarrow, P_{ m lte} \downarrow$
$U_{ m dc}$ -	$E_{\mathrm{sm}} < E_{\mathrm{smmin}}$	$L_{ m ipu} {\uparrow}$	$P_{\rm lce} \downarrow, P_{\rm lse} \downarrow, P_{ m lte} \downarrow$
$U_{ m dc}$ -	$E_{\rm sm} > E_{\rm smmin}$	$L_{ m ipu} {\uparrow}$	$P_{\rm lce}\uparrow, P_{\rm lse}\uparrow, P_{ m lte}\uparrow$

For the H-bridge converter, when the rated output current is determined, its power device losses are positively correlated only with the DC voltage $U_{\rm dc}$.

3. MAIN CIRCUIT PARAMETER DESIGN PROCESSES

The power supply design incorporates appropriate operational margins while accounting for critical constraints including power dissipation limits and control system capabilities. The reference design specifications are summarized in Table 3.

TABLE 3. Design Requirements for EAST Voltage-Source Type Poloidal Field Coil Power Supply

Indicator	Symbol	Design reference requirements
Effective value of the primary side phase current	$I_{ m pe}$	346A
Effective value of the output current	$I_{ m oe}$	15kA
Fundamental frequency amplitude of primary side phase voltage	$E_{ m pm}$	8.164kV
Primary-side phase current harmonic effective value	$hip_{ m av}$	$<2.5\%I_{pe}$ (8.7A)
Output current harmonic effective value	$hio_{ m av}$	<0.1% <i>I</i> _{oe} (15.0A)
DC voltage	$U_{ m dc}$	400V~1000V
Rated total loss of PWM converter power devices	$P_{ m lte_pwm}$	<108kW
Rated total loss of H-bridge converter power devices	$P_{ m lte_hb}$	<72kW
Open-loop amplitude margin	$g_{ m m}$	>6dB
Open-loop phase margin	$p_{ m m}$	30°~60°
Closed-loop control bandwidth	<i>Ф</i> ь	>500Hz
Switching frequency	$f_{ m s}$	1kHz~2kHz
Control cycle	$T_{ m ct}$	50μs

In the parametric design of power supplies,, the harmonic effective value of the current serves as a criticalindicator for evaluating power quality, directly influencing long-term operational stability and thus constituting a key consideration in the design process. First, for a single-branch design, experimental results show that the primary-side phase current harmonic effective value (hip_{av}) is mainly influenced by the modulation index (m_e) and primary-side inductance (L_{ipu}), and is independent of the DC voltage (U_{dc}). The experiments show that, with a fixed U_{dc} , increasing m_e can effectively reduce power device losses and improve system stability margins. Therefore, m_e should be selected as its theoretical maximum value of 1.15. However, considering the U_{dc} drop under dynamic loads, it should be appropriately reduced to 1.05 to ensure system stability. After determining m_e , adjusting L_{ipu} can optimize the harmonic effective value and simplify the design process.

Output current harmonic analysis indicates that, under the premise of meeting the H-bridge output voltage range, reducing $U_{\rm dc}$ helps to lower the output current harmonic effective value. Due to the large inductance of the load, $U_{\rm dc}$ can be selected within the range of 400V to 1000V as the initial design value. For the filter inductance $L_{\rm o}$, since the load inductance is large, its effect can be neglected, and a smaller $L_{\rm o}$ can be chosen in practical applications to meet the current-sharing control requirements.

As indicated in Table 2., once $m_{\rm e}$ and $L_{\rm ipu}$ are determined, adjustment of the $U_{\rm dc}$ serves as an effective means to balance power device losses. Different types of converters have different effects on $U_{\rm dc}$ adjustments, so during the parameter iteration process, $U_{\rm dc}$ should be appropriately adjusted according to loss calculations, or further optimization of power losses can be achieved by adjusting $L_{\rm ipu}$. If the loss control effect is still not ideal, switching frequency can be reduced to decrease losses, though this may lead to increased harmonic effective values, potentially requiring an increase in the number of branches or adjustment of transformer connection groups and carrier phase-shifting angles to meet design requirements.

For cases where $L_{\rm ipu}$ is less than 1, the value of $E_{\rm sm}$ influences both the power device losses and the effective value of the primary-side phase current harmonics. When $E_{\rm sm}$ is smaller than the minimum value, the power device losses are larger, but the current harmonic effective value is more favorable. When $L_{\rm ipu}$ is at its maximum value of 1, $E_{\rm sm}$ should be selected to be at the minimum value to optimize the system's performance. If, after adjusting

HUANG LIANSHENG et al.

Preprint of the conference manuscript

 L_{ipu} , the design reference requirements are still not met, E_{sm} should be adjusted to a value smaller than the minimum.

Based on the analysis of current harmonics and parameters, once m_e , L_{ipu} , and U_{dc} are determined, the impact of the control system's integral coefficient K_{ii} on performance is minimal. By analyzing the open-loop and closed-loop transfer functions of the current loop, the gain margin, phase margin, and bandwidth can be computed, which helps in selecting the appropriate K_{pi} value. If a suitable K_{pi} cannot be selected, the switching frequency can be increased to optimize system performance.

In summary, this paper presents a clear power supply parameter design process as shown in Fig. 2, aiming to optimize both the power supply performance and the current harmonic levels through precise adjustments of key parameters.

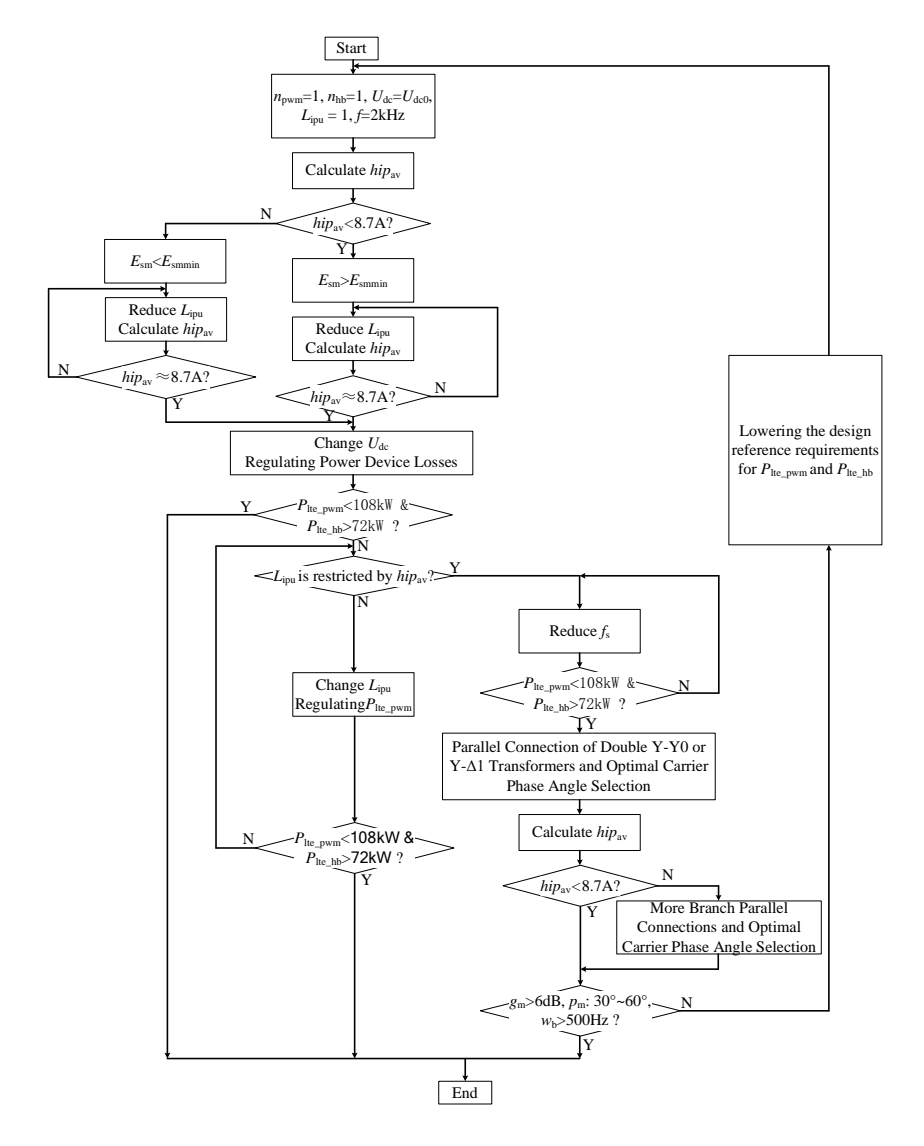


Fig. 2. Flowchart of Parameter Design for EAST Voltage-Source Type Poloidal Field Coil Power Supply

The converter parameters can be obtained through multiple iterative calculations according to the flow chart, as shown in the Table 4.

TABLE 4. Main parameters of the next-generation PFPS

Catagory	Parameter	Value
PFPR	Transformer ration	10 kV / 260 V
	Number of branches	4

IAEA-FEC-2025 / INDICO ID 3240 Preprint of the conference manuscript

	Rated banch power Pej	1.5 MW
	Branch input inductance L_i	70 uH
	DC voltage $U_{\rm dc}$	450 V
	Switching frequency f_{s1}	1 kHz, $T_{s1} = 1 \text{ ms}$
PFHB	Number of branches	4
	Branch output inductance $L_{\rm o}$	70uH
	Switching frequency f_{s2}	1 kHz, $T_{s2} = 1 \text{ ms}$

4. ANALYSIS OF OPERATION RESULTS OF VOLTAGE-SOURCE TYPE POWER SUPPLY

4.1. Power control architecture

The control architecture of the voltage-source poloidal field magnetic coil power supply is illustrated in Fig. 3. The system comprises a master control computer and core control cards (designated as Card 1 and Card 2). Operating on a real-time Linux kernel, the master computer executes sequential processing: it acquires DC voltage and H-bridge output current measurements from ADCs, computes the PWM converter voltage loop and H-bridge output current closed-loop algorithms, generates active current references for the current loop and duty cycle commands for each H-bridge branch, and finally transmits these signals to the core control cards via PCI interface. The core control cards employ a dual-core architecture integrating a ZYNQ XC7Z020 SoC (Xilinx) with an EP4CE15F23I7 FPGA (Altera). Functional distribution is achieved through dedicated assignment - Core Cards 1 and 2 respectively manage distinct converter groups and H-bridge branches, with overall system functionality realized through coordinated operation between the FPGA and ZYNQ's processing system.

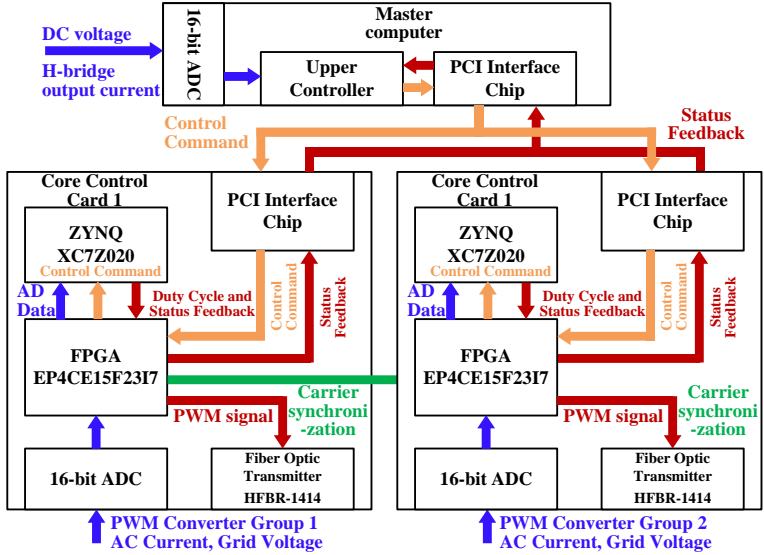


Fig. 3. Schematic Diagram of EAST Voltage-Source Type Poloidal Field Coil Power Supply Control Architecture

4.2. Typical operating waveforms and current harmonic indicators

Fig.4 illustrates the operational waveforms of the voltage-source poloidal field coil power supply during experimental campaigns on EAST. The traces $i_{01} \sim i_{04}$ represent the output currents of the four H-bridge converter branches, while io denotes the total output current. Throughout the depicted operational sequence, the total current io accurately tracks the reference command from the plasma control system, reaching a peak value of 7 kA. The maximum observed current deviation among the individual branches $(i_{01} \sim i_{04})$ is approximately 300 A, corresponding to 8% of the branch rated current. This transient imbalance remains within acceptable operational limits and is rapidly suppressed by the control system, demonstrating negligible impact on overall system performance. These results validate the effectiveness of the circulating current control strategy in the H-bridge converters and confirm the appropriateness of the corresponding parameter design.

HUANG LIANSHENG et al. Preprint of the conference manuscript

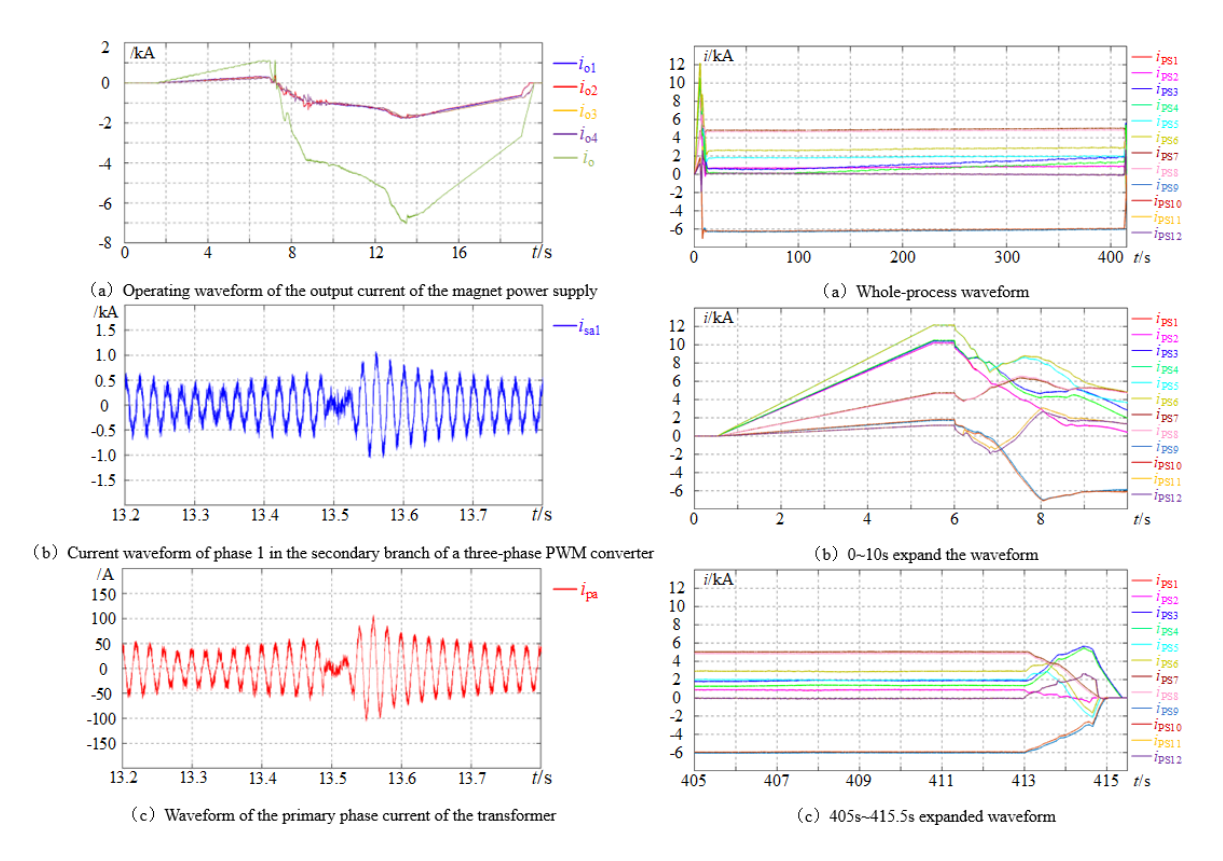


Fig. 4. Typical operating waveform of EAST next-generation poloidal field coil power supply

Fig.5. Operating waveforms of the poloidal field coil power supply in 403-second high-power H-mode

In Fig. 4, $i_{\rm sal}$ represents the phase a current of branch 1 of the PWM converter, and $i_{\rm pa}$ is the phase a current of the transformer primary side. The phase current waveforms are adjusted according to the change in the output current to match the power required by the poloidal field coil. During the adjustment process, the sinusoidal shape of $i_{\rm sal}$ and $i_{\rm pa}$ is clearly maintained without any oscillatory divergence. Due to the real-time change in amplitude, two sets of typical fundamental frequency amplitudes of $i_{\rm sal}$ in Fig. 4, 0.91 kA and 0.5 kA, are selected for current harmonic analysis. The analysis results are summarized in Table 5.

TABLE 5. Results of AC current harmonics under actual operating conditions

$I_{ m smj}$	THD isa1	hisav	$I_{ m pm}$	$\mathrm{THD} i_{\mathrm{pm}}$	hip_{av}
0.91kA	16.35%	105A	96A	9.65%	5A
0.50kA	29.75%	105A	51A	18.03%	6.5A

In Table 5, $I_{\rm smj}$ is the fundamental frequency amplitude of $I_{\rm sal}$, and $I_{\rm pm}$ is the fundamental frequency amplitude of $I_{\rm pa}$. $his_{\rm av}$ is the effective value of the secondary phase current harmonics, and $hip_{\rm av}$ is the effective value of the primary phase current harmonics. Under the influence of carrier phase-shift modulation, the total harmonic distortion (THD) of $i_{\rm pm}$ is significantly smaller than that of $i_{\rm sal}$. $hip_{\rm av}$ is also less than 5% of $I_{\rm pe}$, which meets the design requirements. Based on the above analysis, the operation results further verify the effectiveness of the proposed parameter design method.

4.3. Results of long-pulse operation

On April 12, 2023, the EAST poloidal field power supply supported a 403-second high-power H-mode operation, breaking the world record. The operation results are shown in Fig. 5. $i_{PS1} \sim i_{PS12}$ are the output current waveforms of 12 sets of poloidal field coil power supplies, where $i_{PS1} \sim i_{PS10}$ are the output current waveforms of the second-generation thyristor power supplies, and i_{PS11} and i_{PS12} are the output current waveforms of two sets of next-generation voltage-source poloidal field coil power supplies.

Fig. 5 illustrates the current waveform of the poloidal field coil power supply recorded during a 403-second high-power H-mode (high confinement mode) discharge. The operational sequence comprises the following distinct

IAEA-FEC-2025 / INDICO ID 3240

Preprint of the conference manuscript

phases:

- (a) 0~6 seconds (Premagnetization stage): The power supply operates in forward rectification mode to gradually energize the superconducting poloidal field coil, raising the coil current to a predetermined value set by discharge requirements.
- (b) 6 seconds ~ 6.03 seconds (Plasma current generation stage): Upon reaching the target coil current, the thyristor-based switch in the Switch Network Unit (SNU) is turned off, commutating the loop current into a dump resistor. This action induces a transient voltage of approximately 2400 V across the coil, initiating gas breakdown and plasma formation in the vacuum vessel.
- (c) 6.03 seconds ~ 9 seconds (Plasma current slow rise stage): The SNU thyristor switch is turned on again. At this point, the plasma current slowly rises to the preset flat-top segment under the drive of the converter system.
- (d) 9 seconds ~ 413 seconds (Plasma flat-top stage): The power supply system is in the feedback regulation stage for plasma current, plasma position, and shape. Depending on the requirements of different coils, the power supply system may operate in either the inverter or rectification state, with the current being either positive or negative.
- (e) 413 seconds ~ 415.5 seconds (Plasma current drop stage): When the coil current reaches the predetermined value and the predetermined discharge time is reached, the power supply drives the current of the superconducting coil to slowly decrease to zero, demagnetizing the coil and stopping the system's operation.

Throughout the entire operation process, the voltage-source poloidal field coil power supplies PS11 and PS12 exhibit excellent output current control effects and stable operating performance.

5. CONCLUSION

This paper presents a systematic methodology for parameter design of the next-generation poloidal field coil power supply for the EAST tokamak. Based on the proposed design framework, two full-scale power supply units have been successfully implemented. To date, these systems have consistently operated throughout a two-year experimental campaign supporting EAST experiments, demonstrating robust performance and long-term reliability. The established design approach and operational experience provide a theoretical foundation and technical reference for future development of higher-power coil power supplies.

REFERENCES

- [1] Chen T, Fu P, Chen X, et al. An optimized bidirectional buck–boost converter for DC bus voltage stabilization in new generation poloidal field power supply[J]. Energy Reports, 2022, 8: 188-200.
- [2] Hou M, Qian Y Z, Liu S Q, et al. Design of power supply system for the NanChang Spherical Tokamak[J]. AIP Advances, 2022, 12(2).
- [3] Bigot B. Progress toward ITER's first plasma[J]. Nuclear Fusion, 2019, 59(11): 112001.
- [4] Lieying Y, Weimin X, Huajun L, et al. Design and development of the power supply system for HL-2A tokamak[J]. Fusion engineering and design, 2005, 75: 163-167.
- [5] Zhang M, Shao J, Ma S X, et al. Design of the power supply system for the plasma current modulation on J-TEXT tokamak[J]. Fusion Engineering and Design, 2016, 108: 92-97.
- [6] Barabaschi P, Kamada Y, Shirai H, et al. Progress of the JT-60SA project[J]. Nuclear Fusion, 2019, 59(11): 112005.
- [7] ABakas P, Okazaki Y, Shukla A, et al. Review of hybrid multilevel converter topologies utilizing thyristors for HVDC applications[J]. IEEE Transactions on Power Electronics, 2020, 36(1): 174-190.
- [8] Bakas P, Ilves K, Okazaki Y, et al. Hybrid alternate-common arm converter with high power capability: Potential and limitations[J]. IEEE Transactions on Power Electronics, 2020, 35(12): 12909-12928.
- [9] Wang Z, Fu P, Huang L, et al. Unified power control strategy for new generation poloidal field power supply[J]. Fusion Engineering and Design, 2021, 168: 112404.
- [10] Dou S, Chen X, Huang L, et al. Design of the new generation EAST poloidal field magnet power supply[J]. Fusion Engineering and Design, 2025, 215: 115004.